International Journal of Nanomedicine

Dovepress
open access to scientific and medical research

Open Access Full Text Article

ORIGINAL RESEARCH

3D conductive nanocomposite scaffold for bone tissue engineering

This article was published in the following Dove Press journal:
International Journal of Nanomedicine
24 December 2013
Number of times this article has been viewed

Aref Shahini[1]
Mostafa Yazdimamaghani[2]
Kenneth J Walker[2]
Margaret A Eastman[3]
Hamed Hatami-Marbini[4]
Brenda J Smith[5]
John L Ricci[6]
Sundar V Madihally[2]
Daryoosh Vashaee[1]
Lobat Tayebi[2,7]

[1]School of Electrical and Computer Engineering, Helmerich Advanced Technology Research Center, [2]School of Chemical Engineering, [3]Department of Chemistry, [4]School of Mechanical and Aerospace Engineering, [5]Department of Nutritional Sciences, Oklahoma State University, Stillwater, OK, USA; [6]Department of Biomaterials and Biomimetics, New York University, New York, NY; [7]School of Material Science and Engineering, Helmerich Advanced Technology Research Center, Oklahoma State University, Tulsa, OK, USA

Correspondence: Lobat Tayebi; Daryoosh Vashaee
Helmerich Research Center
700 N Greenwood Ave Tulsa, OK 74106, USA
Tel +1 918 594 8634
Fax +1 270 897 1179
Email lobat.tayebi@okstate.edu; daryoosh.vashaee@okstate.edu

Abstract: Bone healing can be significantly expedited by applying electrical stimuli in the injured region. Therefore, a three-dimensional (3D) ceramic conductive tissue engineering scaffold for large bone defects that can locally deliver the electrical stimuli is highly desired. In the present study, 3D conductive scaffolds were prepared by employing a biocompatible conductive polymer, ie, poly(3,4-ethylenedioxythiophene) poly(4-styrene sulfonate) (PEDOT:PSS), in the optimized nanocomposite of gelatin and bioactive glass. For in vitro analysis, adult human mesenchymal stem cells were seeded in the scaffolds. Material characterizations using hydrogen-1 nuclear magnetic resonance, in vitro degradation, as well as thermal and mechanical analysis showed that incorporation of PEDOT:PSS increased the physiochemical stability of the composite, resulting in improved mechanical properties and biodegradation resistance. The outcomes indicate that PEDOT:PSS and polypeptide chains have close interaction, most likely by forming salt bridges between arginine side chains and sulfonate groups. The morphology of the scaffolds and cultured human mesenchymal stem cells were observed and analyzed via scanning electron microscope, micro-computed tomography, and confocal fluorescent microscope. Increasing the concentration of the conductive polymer in the scaffold enhanced the cell viability, indicating the improved microstructure of the scaffolds or boosted electrical signaling among cells. These results show that these conductive scaffolds are not only structurally more favorable for bone tissue engineering, but also can be a step forward in combining the tissue engineering techniques with the method of enhancing the bone healing by electrical stimuli.

Keywords: conductive polymers, bone scaffold, gelatin, bioactive glass nanoparticles, PEDOT:PSS, conductive scaffold

Introduction

Bone has natural electrical properties such as piezoelectricity, discovered in 1950.[1] These properties create an endogenous electrical field in response to strains that alter cell proliferation.[2] That can explain why external electric and electromagnetic stimulation have progressive influence in bone healing treatment.[3–5] It was shown that such stimulations modify osteoblast activities including adhesion, proliferation,[6] nodule formation,[7] gene expression,[8] protein synthesis,[9] and bone formation markers.[6,10,11]

Ongoing studies in three-dimensional (3D) scaffolds designed for bone tissue engineering are mostly focused on improving the characteristics of the scaffolds in regard to their chemical and mechanical properties.[12–14] In order to combine the tissue engineering techniques with the idea of enhancing the bone healing by electrical stimuli, the electrical property of the scaffolds needs to be adjusted, which was the aim of this paper. The electrical conductivity of the scaffold can be a key property for the

local delivery of applied electrical stimuli. To improve the conductivity of the scaffolds, compositions of biocompatible conductive polymer (CP) were employed.

Since the 1980s, CPs with acceptable biocompatibility have been used in various biomedical applications.[15] CPs mediate electrical stimulation and have the potential to be the stimulating factor that promotes bone regeneration. Previous reports show that the addition of CP can improve the mechanical strength and the biodegradability[16] of scaffolds as well as their in vitro biocompatibility.[17] Although some investigations have been performed recently for producing conductive two-dimensional substrates,[6,11,18,19] composite,[20] and copolymer[21] for bone tissue engineering, to the best of the authors' knowledge, the application of CPs in a porous 3D bone tissue scaffold has not been reported.

Poly(3,4-ethylenedioxythiophene) (PEDOT) is a biocompatible CP which is recently being employed in biomedical applications,[22] especially in nerve tissue engineering.[23] To gain a water soluble polyelectrolyte system with good film-forming properties, PEDOT is doped with poly(4-styrenesulfonate) (PSS).[24] This copolymer has a moderate band gap and good stability in the doping state.[25]

In this study, a new class of bone scaffolds is presented by employing PEDOT:PSS, gelatin (Gel), and bioactive glass nanoparticles (BaG), making a composite of a CP, polypeptide, and ceramic. Gel is a natural polymer with high biocompatibility and biodegradability, which is widely used in tissue engineering scaffolds.[26,27] BaG are biocompatible, osteoconductive, osteoproductive,[28] and capable of bonding with natural bone tissue.[29] The ingredients of Gel and BaG composite mimic the natural organic and mineral constituents of bone, which are collagen fibers and hydroxyapatite crystals.[30] In a recent investigation, the optimized composition of BaG and Gel for bone tissue scaffolds was reported to be 30:10 (weight percent [wt%] in the stock solution).[31] In this study, 0.1%–0.3% of PEDOT:PSS was added to this optimized value. The results indicate that by increasing PEDOT:PSS, conductivity, cell viability, and mechanical properties were enhanced. The scaffolds were fully characterized using Fourier transform infrared spectroscopy (FTIR), X-ray diffraction (XRD), ^{1}H nuclear magnetic resonance (NMR), and swelling, degradation, and porosity measurements as well as differential scanning calorimetry (DSC) and thermal gravimetric analysis (TGA). The morphology of the scaffolds and adult human mesenchymal stem cells (hMSC) cultured on the scaffolds were studied using scanning electron microscopy (SEM), micro-computed tomography, and confocal fluorescent microscopy.

Material and methods

Materials

PEDOT:PSS (1.3 wt% dispersion in water, PEDOT content 0.5 wt%, PSS content 0.8 wt%, conductive grade), BioReagent Gel (from porcine skin, Type A), phosphate buffered saline (PBS) tablets, tetraethyl orthosilicate ($C_8H_{20}O_4Si$), calcium nitrate ($Ca[NO_3]_2 \cdot 4H_2O$), triethyl phosphate ($C_6H_{15}O_4P$), and 0.1 M nitric acid (HNO_3) were purchased from Sigma-Aldrich (St Louis, MO, USA). The crosslinker 1-(3-dimethylaminopropyl)-3-ethylcarbodiimide hydrochloride was purchased from Acros Organics (Geel, Belgium), and N-hydroxysuccinimide ($C_4H_5NO_3$) was purchased from Alfa Aesar (Ward Hill, MA, USA). All other materials were reagent grade.

Preparation of the nanocomposite conductive scaffolds

The sol–gel prepared BaG consisting of silicone dioxide (SiO_2)–phosphorus pentoxide (P_2O_5)–calcium oxide (CaO) (64% SiO_2, 5% P_2O_5, and 31% CaO) (based on mole percentage) was synthesized employing the previously reported method.[32] To obtain a solution of 10% (w/v) Gel, 30% (w/v) BaG, and 0%, 0.1%, and 0.3% (w/w) PEDOT:PSS, the following procedure was performed: Gel and BaG was dissolved in deionized water (10 g Gel and 30 g BaG in 100 mL water). Then PEDOT:PSS was added to the mixture in the amount of 0.1%–0.3% of the total mass of the solution (Table 1). The mixtures were homogenized and degassed by vortexing for 5 minutes and centrifugation (Uni Cyclone UM113; JAPAN UNIX CO., Tokyo, Japan) at 2,000 rpm for 30 minutes.

Prepared conductive nanocomposites were molded and frozen at −20°C for 6 hours. Then they were freeze-dried at −50°C and 1.8 mbar (Labconco, Kansas City, MO, USA) for 24 hours to obtain a porous scaffold. The scaffolds prepared from 0%, 0.1%, and 0.3% (w/w) PEDOT:PSS in the mixture of 10% (w/v) Gel and 30% (w/v) BaG were labeled 0 P, 0.1 P, and 0.3 P, respectively.

Table 1 Concentration of poly(3,4-ethylenedioxythiophene) poly(4-styrene sulfonate), gelatin, and bioactive glass nanoparticles in the aqueous solution

Scaffold	PEDOT:PSS (w/w), %	Gelatin (w/v), %	Bioactive glass (w/v), %
0 P	0	10	30
0.1 P	0.1	10	30
0.3 P	0.3	10	30

Notes: 0 P, 0.1 P, and 0.3 P represent the scaffolds prepared from 0%, 0.1%, and 0.3% (w/w) poly(3,4-ethylenedioxythiophene) poly(4-styrene sulfonate) in the mixture of 10% (w/v) gelatin and 30% (w/v) bioactive glass nanoparticles.

Crosslinking

To gain higher mechanical strength and degradation resistance, the scaffolds were crosslinked by soaking in 50 mM 1-ethyl-3-(3-dimethylaminopropyl)carbodiimide hydrochloride/8 mM N-hydroxysuccinimide/95% alcohol crosslinking solution at 4°C for 48 hours. During the crosslinking of Gel, carbodiimide is a condensation agent used between carboxyl groups and active amine groups to make stable amide bonds.[33] To remove the residual crosslinks, the scaffolds were sonicated in deionized water for 30 seconds and washed with deionized water three times. Figure 1 shows the schematic diagram of preparation of the 3D conductive scaffolds.

Sample characterization

Fourier transform infrared spectroscopy

To analyze the chemical bonding and functional groups, the samples were investigated by FTIR spectroscopy using a Varian 780 IR (Agilent Technologies, Santa Clara, CA, USA). For IR analysis, 1 mg of the ground samples were mixed with 3 mg potassium bromide and analyzed by diffusive powder method in the range of 500–4,000 cm^{-1} with a resolution of 4 cm^{-1} and an average of 40 scans.

Nuclear magnetic resonance

^{1}H high-resolution magic angle spinning (HR-MAS) spectra were taken on a 600 MHz Varian Inova NMR spectrometer (Agilent). An Agilent solid-state HXY 3.2 mm MAS probe was used. The probe was tuned to $^{1}H/^{13}C/2H$, and the ^{2}H channel was used for locking. 0 P and 0.3 P scaffolds soaked in heavy water (D_2O) were cut with a punch to the inner diameter of the rotor. Several punched pieces were placed firmly in the sample region of a rotor with silicone disc and O-ring spacers for liquid containment obtained from Revolution NMR, LLC (Fort Collins, CO, USA). The spinning speed of the rotor was adjusted to 5±0.2 kHz. ^{1}H HR-MAS one-pulse spectra of the gels were taken with a 90 degree pulse of 4.5 μseconds delay between scans of 2 seconds, and 128 scans, while controlling the temperature at 25°C. The water peak at 4.79 ppm was used as reference. Data were transformed and plotted using the MestReNova program from Mestrelab Research (Santiago de Compostela, Spain).

X-ray diffraction

XRD analysis on the scaffolds was accomplished employing a Bruker D8 Discover system (Bruker Corporation, Billerica,

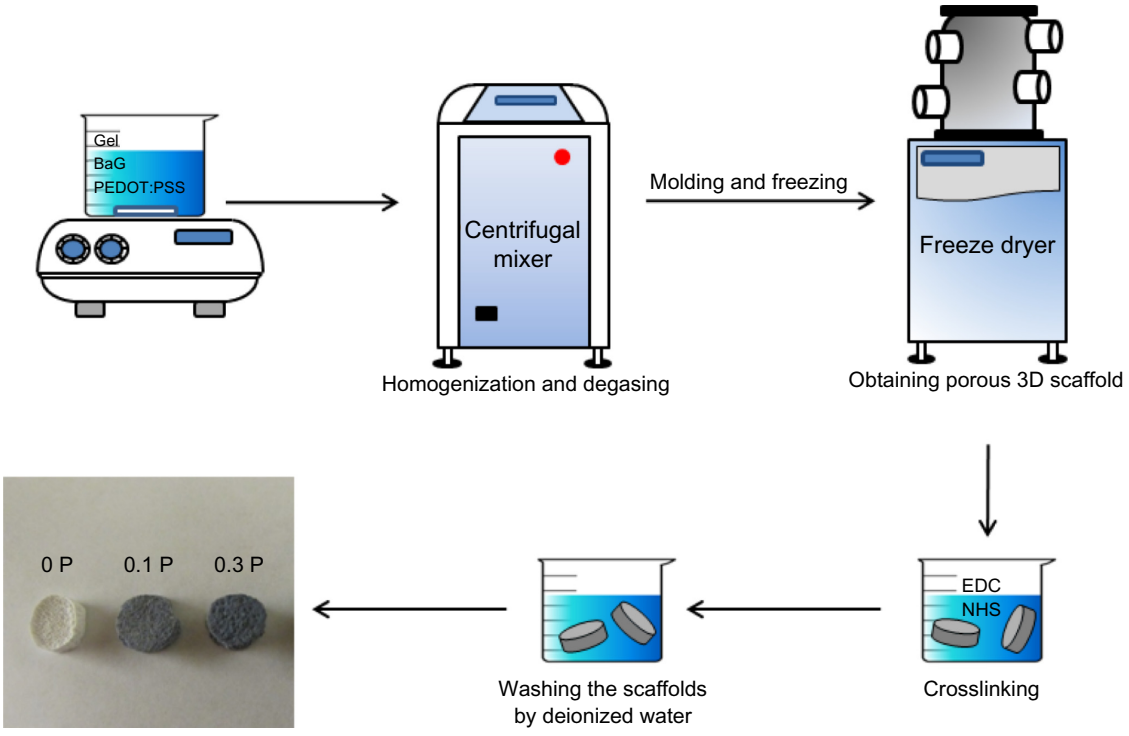

Figure 1 Schematic diagram of the preparation of three-dimensional scaffolds with the freeze-drying method.
Notes: 0 P, 0.1 P, and 0.3 P represent the scaffolds prepared from 0%, 0.1%, and 0.3% (w/w) poly(3,4-ethylenedioxythiophene) poly(4-styrene sulfonate) in the mixture of 10% (w/v) gelatin and 30% (w/v) bioactive glass nanoparticles.
Abbreviations: 3D, three dimensional; BaG, bioactive glass nanoparticles; EDC, 1-(3-dimethylaminopropyl)-3-ethylcarbodiimide hydrochloride; Gel, gelatin; NHS, N-hydroxysuccinimide; PEDOT:PSS, poly(3,4-ethylenedioxythiophene) poly(4-styrene sulfonate).

MA, USA) to identify the diffraction pattern of the scaffolds. This instrument uses copper Kα radiation (λ=1.54056 Å) and works with voltage of 40 kV and current settings of 40 mA. XRD diagrams were recorded for $20 \leq 2\theta \leq 70$.

Morphological and microstructure analysis

The morphology and microstructure of the scaffolds were observed via SEM. To see the cross section view of the scaffolds, they were cut using a double edge razor blade. The scaffolds were gold coated by sputtering (SPI Module™ Sputter Coater; Structure Probe, Inc, West Chester, PA, USA), and then were structurally evaluated by performing SEM using a Hitachi S-4800 (Hitachi Ltd, Tokyo, Japan) with voltage and amperage of 20 kV and 2 μA. The pore sizes of the scaffolds were measured by analyzing SEM micrographs employing ImageJ software (Sun Microsystems, Inc., Santa Clara, CA, USA).

To observe the 3D structure of the scaffolds, micro-computed tomography imaging was employed. Scaffolds were scanned (SCANCO Medical AG, Brütisellen, Switzerland) at a resolution of 2,048 × 2,048 pixels or 6 μm thick slices. Semi-automated contours were placed so that the total structure of the scaffold could be visualized. Following reconstruction, 3D images of the scaffolds were generated.

The 3D images of cells on scaffolds were collected using a confocal microscope (Leica TCS SPE; Leica Microsystems, Wetzlar, Germany). HCX PL APO CS 20.0 × 0.70 DRY UV objective was employed and the laser beam was activated for 488 nm wavelength excitation. Fluorescent image stacks of cytoplasmic carboxyfluorescein diacetate succinimidyl ester (CFDA-SE) at 517 nm emission along the z-axis were collected at a step size of 1 μm. The observed thickness of the z-axis was 100 μm. The format of images was adjusted at 512 × 512 with a speed of 400 Hz, zoom factor of 1.5, frame average of one, accuracy of one, and a gain of 900 V. Leica Application Suite Advanced Fluorescence (LAS AF) software version 2.6 (Leica Microsystems) was used for image processing.

Obtained micrometer scale images showed the morphology of the different scaffolds, the average size of pores and quality of cell attachment on the structure of the scaffold.

Swelling measurement

The water uptake or swelling analysis was performed on five specimens of each scaffold (diameter 9 mm, thickness 2 mm, and mass ~50 mg). After measuring the dry weight of test specimens (W_d), they were immersed in PBS (pH =7.4) at a constant temperature (37°C) for predetermined time intervals, and wet weights (W_w) were determined at these time intervals after removing excess surface water by tissue paper. The swelling ratios (S) of the specimens were calculated using the following equation:

$$S = \frac{(W_w - W_d) \times 100}{W_d}. \quad (1)$$

Degradation measurement

In vitro biodegradation of scaffolds was analyzed by incubating the scaffolds in an enzymatic solution of 0.1 mg/mL collagenase in PBS and measuring their weight loss at different incubation times. The scaffolds were cut to three specimens with 30 mg weight (W_a). They were sterilized in 70% ethanol for 15 minutes and washed three times with sterile PBS. Then they were immersed in 25 mL of the enzymatic solution. At predetermined time intervals, the scaffolds were removed from the solution and were dried in a vacuum to measure the residual weight (W_b). The weight loss or degradation rate was calculated using the following equation:

$$\text{Weight loss (degradation rate)} = \frac{(W_a - W_b) \times 100\%}{W_a}. \quad (2)$$

Weight loss is a measure of scaffold degradation and indicates the weight of materials left in the bulk of the scaffolds compared to its original mass. For example, 50% weight loss means only half of the original mass of the scaffold remains in the bulk scaffold; 100% degradation indicates the complete collapse of the scaffold.

Porosity measurement

The porosity of scaffolds was determined by the ethanol replacement method.[34] Three specimens of each scaffold were chopped in a cylindrical shape with radius and thickness of 4.5 mm and 2.0 mm, respectively. After measuring their initial weight, the scaffolds were immersed in 20 mL ethanol and subsequently treated with an evacuation–repressurization system until no more bubbles came out of the specimens. The ethanol-absorbed specimens were weighed after wiping with tissue paper. The porosity of scaffolds was calculated using the following equation:

$$\text{Porosity} = \frac{(W_w - W_d) \times 100\%}{\rho_{et} \times \pi R^2 T} \quad (3)$$

where W_w is the weight of ethanol-absorbed scaffolds, W_d is the weight of dry scaffolds, ρ_{et} is ethanol density, R is the radius, and T is the thickness of the scaffolds.

Cell culture

Adult hMSC were purchased from Lonza Walkersville, Inc (Walkersville, MD, USA) and cultured in mesenchymal stem cell basal medium (MSCGM™; Lonza Walkersville, Inc) with other supplements as recommended via protocol (Lonza Walkersville, Inc). Cells were incubated at 37°C and 5% carbon dioxide/95% air atmosphere and medium was exchanged every 3–4 days. Cultures proliferated normally in the manner of size, shape, and confluency. Upon confluency, the cells were removed from the plate with Clonetics™ trypsin/ethylenediaminetetraacetic acid (Lonza Walkersville, Inc). Cells then underwent centrifugation at 300 g for five minutes and were suspended in growth medium. Viable cell counting was conducted using Trypan blue dye exclusion assay. Next, the cells were stained using an amine-reactive, colorless, nonfluorescent dye that diffuses into the cytoplasm of cells, 5-(and-6)-CFDA-SE mixed isomers obtained from Life Technologies (Carlsbad, CA, USA).

All scaffolds were sterilized under ultraviolet for 24 hours in a laminar hood and placed in a 24-well plate precoated with bovine serum albumin to minimize direct attachment of cells to the plate. Quadruplicate samples were used for each condition. Then, 1×10^4 cells were seeded onto a tissue culture plastic surface and each scaffold for viability analysis and 2×10^4 cells were seeded for microscopy samples. To achieve a uniform distribution of cells in four scaffolds, a concentrated (500,000 cells/mL) cell suspension was placed at different locations on each scaffold and allowed to attach for 30 minutes prior to adding growth medium. After 1 day, cell-containing scaffolds were fixed in 3.7% formaldehyde for 30 minutes at room temperature.

Scaffolds were also dehydrated using ethanol followed by a brief vacuum drying. Scaffolds were sputter coated with gold at 20 mA prior to observation under SEM.

Quantification of cell viability

Cell viability after 1 day was assessed by two approaches. First, 100 µL spent media collected on that day were used to analyze cell viability indirectly. Second, scaffolds containing cells were washed in MSCGM, and cytoplasmic CFDA-SE stain was extracted from live cells by three cycles of repeated freezing and thawing. CFDA-SE content in the spent medium and the cytoplasm were assessed by fluorescence intensity in Gemini XS spectrofluorometer (Molecular Devices LLC, Sunnyvale, CA, USA) at excitation and emission wavelengths of 485 nm and 525 nm, respectively. Fluorescence intensity of the tissue culture plastic was used as a control.

Thermal analyses

Thermal properties of pure Gel and 0 P and 0.3 P scaffolds were analyzed by TGA and DSC analyses in order to identify any thermal events like decomposition and residual weight of the material. About 15 mg of the ground, dried samples in an alumina crucible were analyzed with STA 449 F1 Jupiter® (NETZSCH-Gerätebau GmbH, Selb, Germany) at a heating rate of 5 K/minute from 25°C to 600°C.

Conductivity measurement

Conductivity of the scaffolds was measured using a 2100 Digital Multimeter (Keithley Instruments, Inc, Cleveland, OH, USA). Two steel blades were planted on a nonconductive substrate with 1 mm distance from each other. Hydrated scaffolds with a thickness of 1 mm and a diameter of 9 mm were placed inside the vacant space between the two blades. Resistance measurement (R) was carried out ten times for three specimens of each sample and the conductivity (δ) was calculated by Pouillet's law equation:

$$\sigma = \frac{L}{R \times A} \tag{4}$$

where L is thickness, D is diameter, and A is the surface area of samples, $A = \pi \times (D/2)^2$.

Mechanical analysis

The stiffness of composite scaffolds was characterized by performing compressive experiments using a rheometer (DHR-2; TA Instruments, New Castle, DE) with normal force accuracy of 5 mN and displacement precision of 1 µm. A 7/32 inch (~5.55 mm) trephine was used to obtain circular disks from a sheet of PEDOT:PSS scaffolds. The specimens were soaked in PBS solution for about 10–12 hours before mechanical tests. The scaffold dimensions were measured with a digital caliper. The submersion chamber of the rheometer was filled with the PBS solution and the scaffolds were compressed between top and bottom loading plates. The compressive stress was calculated by dividing the recorded force by the initial area of specimens. The stress–strain curve was plotted and the secant compressive modulus E was calculated. Three samples for each group were tested, and mean and standard deviation of the measurements were reported.

Results

Fourier transform infrared spectroscopy analysis

The chemical structure of the PEDOT:PSS is depicted in Figure 2A. Figure 2B compares the FTIR spectra of

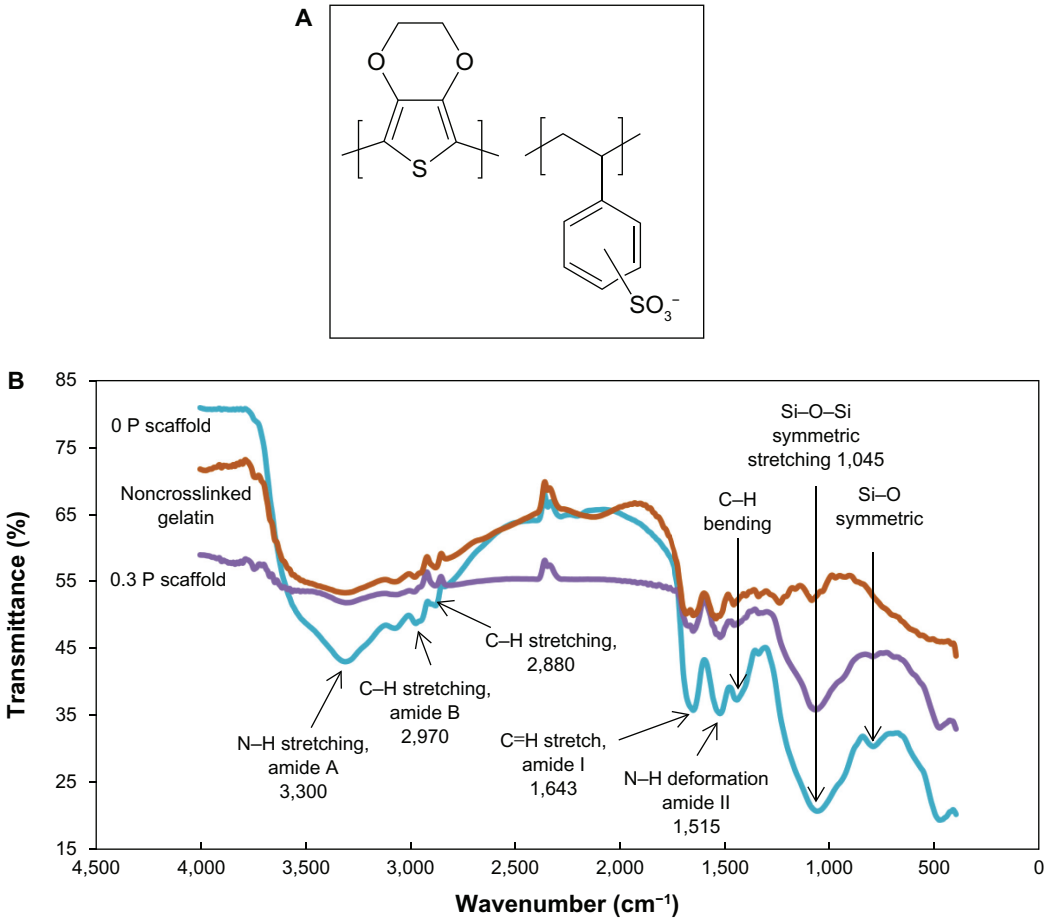

Figure 2 (**A**) Chemical structure of poly(3,4-ethylenedioxythiophene) poly(4-styrene sulfonate). (**B**) The Fourier transform infrared spectroscopy spectra of noncrosslinked gelatin, 0 P, and 0.3 P scaffolds. More intense peaks of amide bonds in the gelatin spectra can be related to crosslinking of carboxyl and amine groups. The presence of bioactive glass nanoparticles is indicated by the silicon peaks.

Notes: 0 P and 0.3 P represent the scaffolds prepared from 0% and 0.3% (w/w) poly(3,4-ethylenedioxythiophene) poly(4-styrene sulfonate) in the mixture of 10% (w/v) gelatin and 30% (w/v) bioactive glass nanoparticles.

noncrosslinked Gel and 0 P and 0.3 P scaffolds. Gel is characterized with amide peaks (N–H bond deformation for amide II at 1,540, C=O stretch for amide I at 1,680, C–H stretch for amide B at 2,975 and N–H stretch for amide A at 3,320). It is suspected that more intense peaks of amide bonds for crosslinked samples might be a sign of bond formation between amine and carboxylic groups which form the bridge bonds. The addition of BaG to Gel shows two peaks for silicon oxide network at 1,050 cm^{-1} and 790 cm^{-1}, which are assigned to Si–O–Si symmetric stretching and symmetric stretching of bridging oxygen between tetrahedrons of the Si–O network, respectively.[28] Due to the low concentration of PEDOT:PSS, the IR absorption of the sulfonic acid group of PSS at 1,225 cm^{-1}, ethylenedioxy group stretching vibration at 1,053 cm^{-1}, C–S stretching at 935 cm^{-1} and 836 cm^{-1}, C–S–C deformation at 692 cm^{-1}, C–O–C stretching at 1,090 cm^{-1} and 1,234 cm^{-1}, and the C–C and C=C stretching of the quinoidal structure at 1,360 cm^{-1} of PEDOT are completely covered by broad absorption of the Si–O network of BaG nanoparticles.[35,36] The FTIR spectrum of the 0.1 P scaffold was similar to that of the 0.3 P scaffold.

^{1}H nuclear magnetic resonance spectra analysis

The ^{1}H HR-MAS NMR spectra of hydrated nonconductive and conductive scaffolds (0 P and 0.3 P) obtained to evaluate the molecular interaction between PEDOT:PSS and Gel polymer chains are shown in Figure 3. Lower amplitude was observed for most of the Gel resonances in the 0.3 P scaffold compared to the 0 P scaffold, while the resonance of water had greater intensity for the 0.3 P scaffold (not shown in Figure 3 due to the scale). These observations are most likely related, with the increased amount of water in the 0.3 P scaffold corresponding to an effective dilution of the Gel resonances. Since a variable amount of water could have been associated with each scaffold by the method of packing,

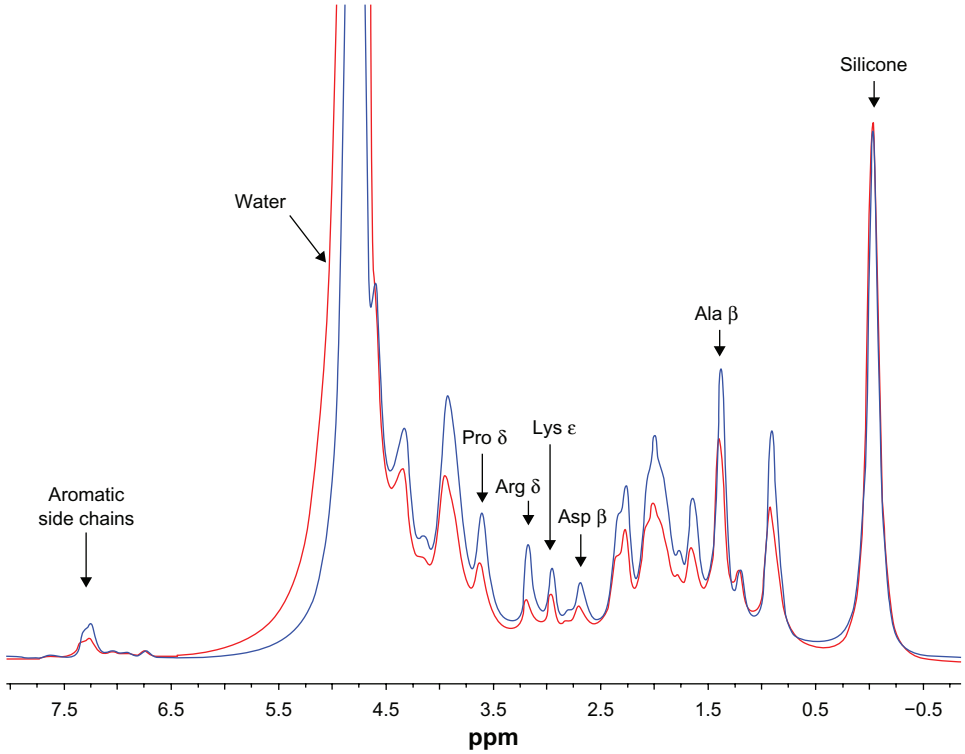

Figure 3 ^{1}H high-resolution magic angle spinning nuclear magnetic resonance spectra of 0 P (blue) and 0.3 P (red) scaffolds soaked in heavy water (D_2O). Peak assignments for gelatin follow Rose and Gross.[62] Silicone resonance is due to disc and O-rings in the magic angle spinning rotor. Gelatin resonances have lower amplitude for the 0.3 P scaffold compared to the 0 P scaffold. The peak height of arginine δ significantly decreased with the addition of poly(3,4-ethylenedioxythiophene) poly(4-styrene sulfonate), suggesting that poly(3,4-ethylenedioxythiophene) poly(4-styrene sulfonate) molecules are in close interaction with arginine side chains of gelatin.
Notes: 0 P and 0.3 P represent the scaffolds prepared from 0% and 0.3% (w/w) poly(3,4-ethylenedioxythiophene) poly(4-styrene sulfonate) in the mixture of 10% (w/v) gelatin and 30% (w/v) bioactive glass nanoparticles.

these differences were not considered significant. The one notable difference between the two spectra is that the relative peak heights of the best-resolved side chain resonances arginine δ, lysine ε, and aspartate β differ, with the arginine δ intensity lower than the lysine ε intensity in the spectrum for the 0.3 P scaffold.

The increase of water peak height by having PEDOT:PSS could be related to the hydrophilic nature of the scaffolds.

It may be concluded that by having PEDOT:PSS in the scaffold composition, more bonds are involved in the structure of the composite. This increases the stability of the scaffolds and decreases the height of some of the main NMR peaks. Other experimental results, such as degradation analysis and mechanical property measurement are in line with this hypothesis.

X-ray diffraction analysis

The XRD patterns of scaffolds (Figure 4) did not show any diffraction peaks, indicating the disorder and glassy nature of BaG used in the conductive scaffolds and no crystallization in the BaG/Gel PEDOT:PSS nanocomposite.

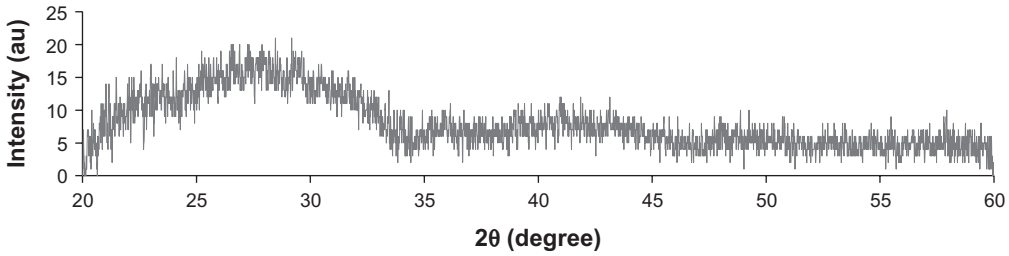

Figure 4 The X-ray diffraction pattern of the 0.3 P scaffold. No diffraction peak in the spectra indicates an amorphous structure of bioactive glass nanoparticles in the composition.
Notes: 0.3 P represents the scaffolds prepared from 0.3% (w/w) poly(3,4-ethylenedioxythiophene) poly(4-styrene sulfonate) in the mixture of 10% (w/v) gelatin and 30% (w/v) bioactive glass nanoparticles.

Structural and pore size analysis

The porosity and pore size of scaffolds are shown in Table 2. The porosity percent was approximately 60% with a slight increase due to the presence of PEDOT:PSS in the composite. The average pore size decreased from 200 µm for 0 P to 110 µm and 160 µm for 0.1 P and 0.3 P, respectively.

Micro-computed tomography 3D imaging and SEM observation from the top view in high and low magnification was carried out to study the morphology of the scaffolds in 3D (Figure 5). The observations showed an interconnected network of spherical pores with high porosity for all scaffolds. The presence of PEDOT:PSS decreased the pore size in the 0.1 P scaffold in comparison with the 0 P scaffold. However, higher concentration of PEDOT:PSS led to an increase of the pore size in 0.3 P compared to the 0.1 P scaffold.

Cell viability and attachment

Viability of hMSC on various structures was evaluated using CFDA-SE stain present in the cytoplasm after 1 day of seeding. Previously, the authors have shown that viability can be accurately assessed by prestaining the cells with CFDA-SE and measuring the cytoplasmic content at a predetermined time.[37] Also, cell division could be tracked using CFDA-SE and flow cytometry. Cytoplasmic content depicts the viable cells present in the scaffolds. Based on the same concept, the cytoplasmic content collected from the freeze thaw cycle was measured for CFDA-SE content. Figure 6A shows an increase in the number of viable cells in all of the scaffolds in comparison to the tissue culture plastic. The viability results also indicate enhancement in the cell attachment and viability with an increase in the concentration of PEDOT:PSS.

To observe cell morphology on the scaffolds, SEM and confocal fluorescent microscopy were employed. These results showed that cells on the scaffolds exhibited stretched shapes in all the scaffolds (Figure 6B and E).

Table 2 Porosity and pore size analysis for different concentrations of poly(3,4-ethylenedioxythiophene) poly(4-styrene sulfonate) in bioactive glass nanoparticles/gelatin poly(3,4-ethylenedioxythiophene) poly(4-styrene sulfonate) composite scaffolds

Scaffold	Porosity, volume %	Pore size (average), µm
0 P	60±5	110–280 (200)
0.1 P	62±6	70–150 (110)
0.3 P	63±5	50–250 (160)

Notes: 0 P, 0.1 P, and 0.3 P represent the scaffolds prepared from 0%, 0.1%, and 0.3% (w/w) poly(3,4-ethylenedioxythiophene) poly(4-styrene sulfonate) in the mixture of 10% (w/v) gelatin and 30% (w/v) bioactive glass nanoparticles.

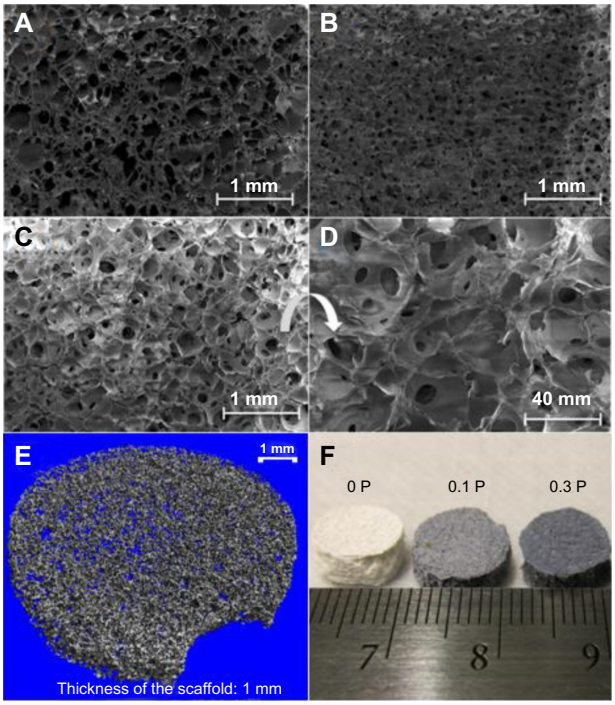

Figure 5 Scanning electron micrograph of the (**A**) 0 P, (**B**) 0.1 P, and (**C**) 0.3 P scaffolds, and the (**D**) 0.3 P scaffold at high magnification. (**E**) Micro-computed tomography image of the 0.3 P scaffold and (**F**) overall view of the scaffolds. The interconnected network of spherical pores with an average size of 100–200 µm provides a good environment for cell migration and facilitates the diffusion of nutrients.
Notes: 0 P, 0.1 P, and 0.3 P represent the scaffolds prepared from 0%, 0.1%, and 0.3% (w/w) poly(3,4-ethylenedioxythiophene) poly(4-styrene sulfonate) in the mixture of 10% (w/v) gelatin and 30% (w/v) bioactive glass nanoparticles.

Furthermore, the hMSC were uniformly spread on the scaffolds (Figure 6D and E). Cells showed numerous lamellipodia and filopodia with anchorage points to the conductive scaffold.

Thermal analysis

TGA and DSC thermoanalytical techniques were employed to assess the thermal characteristics of the composite. TGA and DSC plots are depicted in Figure 7 and critical points are marked. These plots show four thermal stages. The first stage is related to the loss of water between 25°C–160°C. Water constituted approximately 3 wt% of the composite and the endothermic peak initiated at 80°C confirms the energy absorption of water evaporation. The second stage is Gel decomposition, in which an endothermic peak started at 200°C and weight loss occurred between 250°C–300°C (~4% weight loss). Passing 300°C, the third stage showed up by a sudden decrease in the slope of the DSC curve due to a consumption of energy, which seems to be related to the endothermic pyrolysis reaction of polypeptide. In the fourth stage, the exothermic peak of the oxidative degradation of Gel occurred at 360°C. This oxidation can be due to the

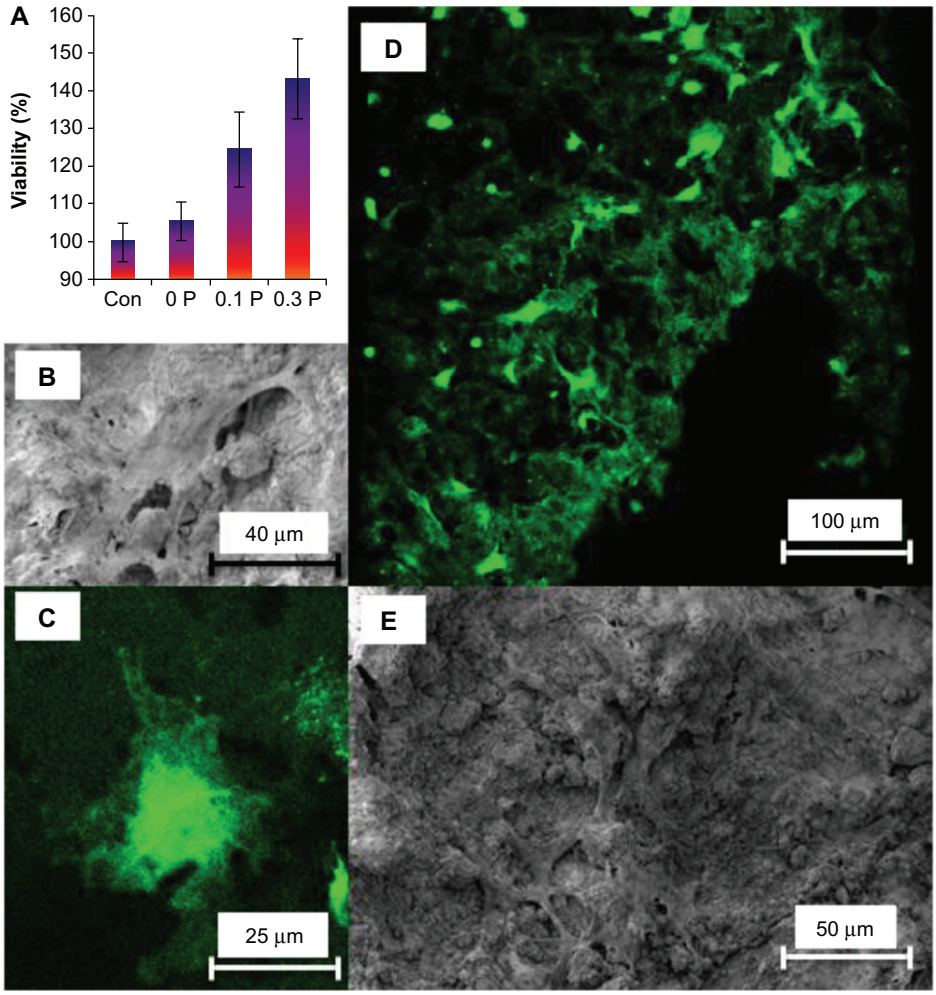

Figure 6 (**A**) Cytoplasmic content of human mesenchymal stem cells on the 0 P, 0.1 P, and 0.3 P scaffolds in comparison to tissue culture plastic (control sample) shows that the number of viable cells increases by increasing the poly(3,4-ethylenedioxythiophene) poly(4-styrene sulfonate) concentration in the composition of scaffolds. The values are mean ± standard deviation (number of samples =3). (**B**) Scanning electron microscopy and (**C**) confocal fluorescent microscopy images of a cell on the 0.3 P scaffold. (**D**) Scanning electron microscopy and (**E**) confocal fluorescent image of cell distribution on the 0.3 P scaffold. Enhanced cell attachment is observed for the conductive scaffolds.

Notes: 0 P, 0.1 P, and 0.3 P represent the scaffolds prepared from 0%, 0.1%, and 0.3% (w/w) poly(3,4-ethylenedioxythiophene) poly(4-styrene sulfonate) in the mixture of 10% (w/v) gelatin and 30% (w/v) bioactive glass nanoparticles.

Abbreviation: con, control.

reaction of Gel with the atmospheric oxygen trapped in the pores of the scaffold. A small shift for all the peaks in 0.3 P compared to 0 P is also observable in the plot.

Swelling behavior and in vitro enzyme degradation analysis

Swelling behavior and degradation results of the scaffolds are pictured in Figure 8. Final swelling percentages of the scaffolds varied in the range of 200–240 wt%. No significant change was observed in the swelling behavior of the different scaffolds. Meanwhile, the volume of scaffolds did not change during swelling.

The degradation of scaffolds was investigated in the collagenase enzymatic solution. The degradation result demonstrated that incorporation of PEDOT:PSS highly influences the degradation behavior of the scaffolds. The presence of PEDOT:PSS enhanced the stability and biodegradation resistance of the scaffolds. While the scaffolds without PEDOT:PSS content were completely degraded in 10 days, the scaffolds with a small percentage of PEDOT:PSS were degraded less than 40% in 90 days.

Electrical properties of BaG/Gel PEDOT:PSS scaffolds

The conductivity of hydrated BaG/Gel/PEDOT:PSS scaffolds is shown in Figure 9. The conductivity increased with addition of PEDOT:PSS to the BaG/Gel composite up to 170 µS/m for the 0.3 P scaffold.

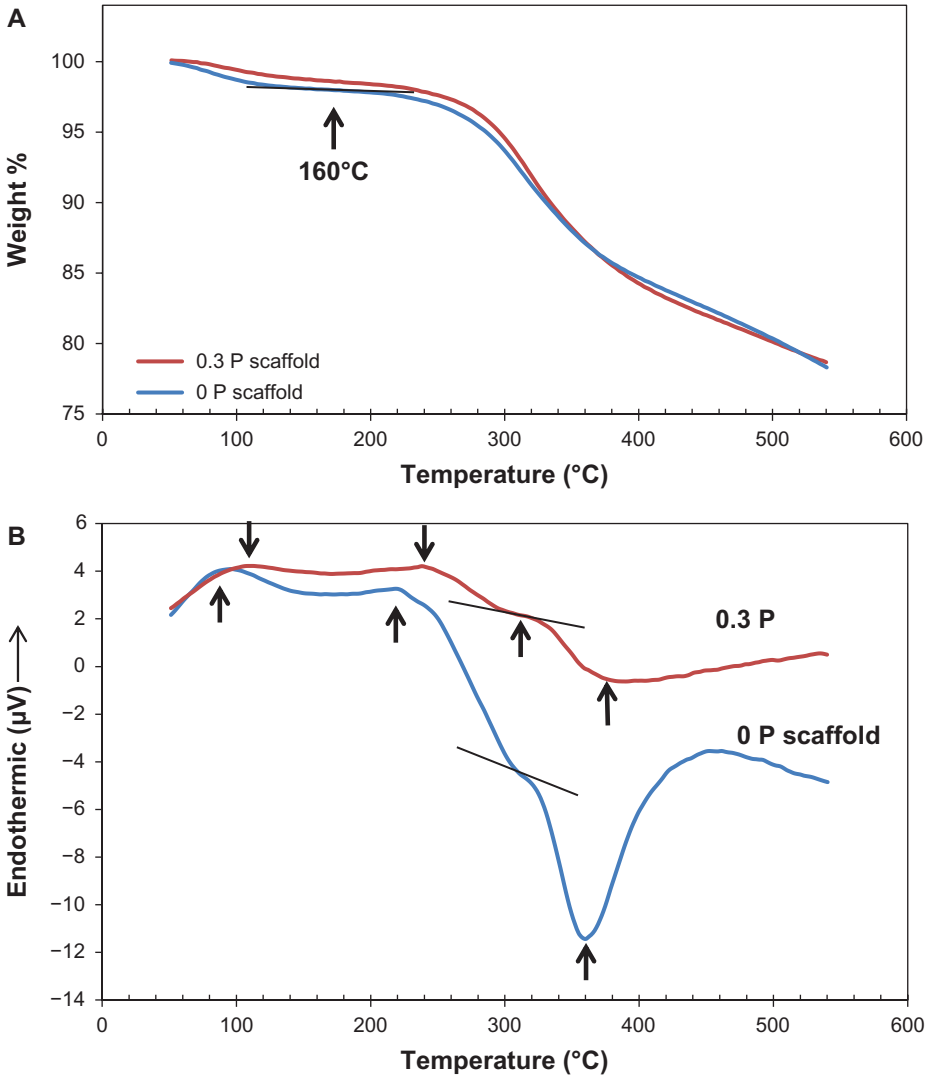

Figure 7 (**A**) Thermal gravimetric analysis and (**B**) differential scanning calorimetry curves of the 0 P and 0.3 P scaffolds. Four thermal stages can be observed in the differential scanning calorimetry plot (water loss, decomposition, pyrolysis, and oxidative degradation). The location of the peaks shows a slight shift to the right for the 0.3 P scaffold.
Notes: 0 P and 0.3 P represent the scaffolds prepared from 0% and 0.3% (w/w) poly(3,4-ethylenedioxythiophene) poly(4-styrene sulfonate) in the mixture of 10% (w/v) gelatin and 30% (w/v) bioactive glass nanoparticles.

Mechanical properties

Table 3 presents the secant compressive modulus of the scaffolds obtained by mechanical compression testing. As can be seen in this table, the average elastic modulus in immersed condition was within 13–35 MPa and increased by increasing the percentage of PEDOT:PSS. Table 3 also compares mechanical properties of BaG/Gel/PEDOT:PSS nanocomposites with those of the spongy bone.

Discussion

The objective of this study was to fabricate a conductive scaffold for bone tissue engineering. The ultimate purpose of making conductive scaffolds is applying effective electrical/magnetic stimuli during bone healing using tissue engineering techniques. As the first step to reach this goal, the authors made the conductive scaffolds by including PEDOT:PSS CP in the composition of BaG/Gel scaffolds that were optimized previously.[31] It was realized that the addition of PEDOT:PSS can improve various characteristics of the scaffolds including physiochemical stability, mechanical strength, and cell attachment.

Since the amount of PEDOT:PSS is significantly smaller than the amount of Gel in the scaffolds and also in the stock aqueous PEDOT:PSS solution, PEDOT must associate strongly with PSS to make it water soluble,[24,38] it may be concluded that grains of PEDOT:PSS were distributed through the BaG/Gel matrix. The PEDOT chains are isolated by PSS chains making a homogenous conductive

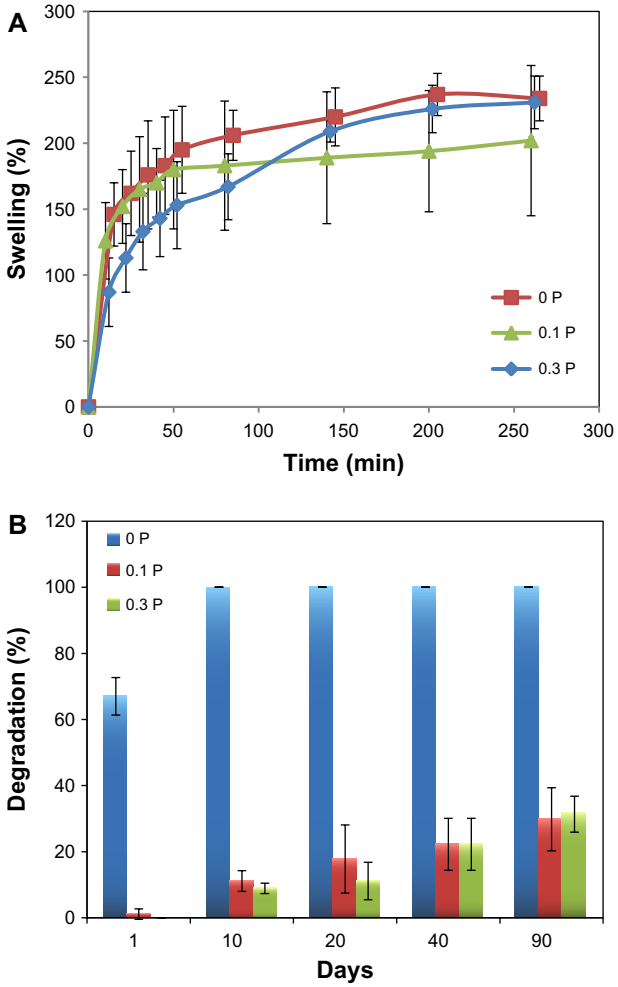

Figure 8 (**A**) Swelling and (**B**) in vitro enzyme degradation analysis of the 0 P, 0.1 P, and 0.3 P scaffolds. Although the presence of poly(3,4-ethylenedioxythiophene) poly(4-styrene sulfonate) did not change the swelling behavior significantly, it dramatically influenced the biodegradation resistance of scaffolds.
Notes: 0 P, 0.1 P, and 0.3 P represent the scaffolds prepared from 0%, 0.1%, and 0.3% (w/w) poly(3,4-ethylenedioxythiophene) poly(4-styrene sulfonate) in the mixture of 10% (w/v) gelatin and 30% (w/v) bioactive glass nanoparticles.

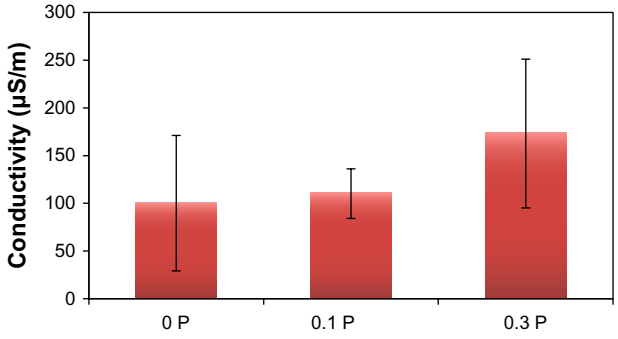

Figure 9 The electrical conductivity of scaffolds is increased by the addition of poly(3,4-ethylenedioxythiophene) poly(4-styrene sulfonate). A 70% increase in conductivity was measured in scaffolds with 0.3% poly(3,4-ethylenedioxythiophene) poly(4-styrene sulfonate).
Notes: 0 P, 0.1 P, and 0.3 P represent the scaffolds prepared from 0%, 0.1%, and 0.3% (w/w) poly(3,4-ethylenedioxythiophene) poly(4-styrene sulfonate) in the mixture of 10% (w/v) gelatin and 30% (w/v) bioactive glass nanoparticles.

Table 3 Mechanical properties of conductive nanocomposites in comparison with spongy bone

Scaffold	Secant modulus (E), MPa	Density (ρ), g/cm³	(E/ρ)
Spongy bone	12–500	0.14–1.2	500
0 P	13±2	0.415±0.070	31
0.1 P	22±1	0.388±0.056	56
0.3 P	35±1	0.367±0.010	95

Notes: Poly(3,4-ethylenedioxythiophene) poly(4-styrene sulfonate) improves the secant modulus of bioactive glass nanoparticles/gelatin scaffold to the range of spongy bone. 0 P, 0.1 P, and 0.3 P represent the scaffolds prepared from 0%, 0.1%, and 0.3% (w/w) poly(3,4-ethylenedioxythiophene) poly(4-styrene sulfonate) in the mixture of 10% (w/v) gelatin and 30% (w/v) bioactive glass nanoparticles.

core in the grains.[38–40] Since the hydrophilic PSS shell is on the outside of a grain, it interacts most closely with the surrounding Gel.

Incorporation of PEDOT:PSS in the composition of the BaG/Gel scaffold increased the chemical stability of the composite. Degradation analysis showed that incorporation of PEDOT:PSS improves the biodegradability resistance of the composite. These results can be related to the chemical stability in the structure of the scaffolds containing PEDOT:PSS. As another outcome of such stability, the mechanical properties (both the secant modulus and the specific secant modulus) were improved by increasing PEDOT:PSS. These results are in agreement with previous studies on biomolecules and CPs in different contexts, which indicated that functional groups of CPs and their dopants led to binding of polypeptides, immobilization of biomolecules, and protein stabilization.[23]

Lysine and arginine side chains of the Gel polypeptide contain ammonium and guanidinium groups, respectively. Due to the high pK_a of these groups (arginine pK_a~12; lysine pK_a~10.5), the lone pair electrons of nitrogen are normally protonated by H^+. Positive protonated amine could electrostatically attract the negatively charged sulfonate groups of PSS, allowing the formation of salt bridges with hydrogen bonds. Since two N–H groups of the guanidinium can simultaneously form hydrogen bonds with two oxygen atoms of the sulfonate,[41,42] the arginine–guanidinium group can form stronger bonds with sulfonate than the lysine ammonium group. Also, as the pK_a for arginine is higher than that of lysine, there is more probability for this side chain to stay in the protonated state and form salt bridges with negatively charged sulfonate in the CP. The ^{1}H HR-MAS NMR spectra showed a greater decrease for the arginine δ than for the lysine ε proton peak amplitude in 0.3 P, suggesting that the side chain of arginine experiences a decrease in flexibility

and so has greater tendency to form a salt bridge with a sulfonate group than does the lysine side chain. Thus, the NMR spectra may propose that the polymer chains of the outer PSS molecules of PEDOT:PSS grains are in close contact with the polypeptide, at least in some arginine residues.

As shown in Figure 9, increase in the PEDOT:PSS concentration in the scaffold resulted in an increase in the conductivity from 100 μS/m for the 0 P scaffold to 170 μS/m for the 0.3 P scaffold. This 70% increase in the conductivity can be due to the charge carrier (hole) motion in the PEDOT:PSS grains that are dispersed in the structure of the conductive scaffolds.

The conductive scaffolds are bioactive and may enhance cell metabolism. According to the cell viability experiments, an increase in the cytoplasmic content of the cells on the conductive scaffolds suggests that they are suitable for cell attachment and proliferation. Enhanced extracellular matrix traces were reproducibly observed in the conductive scaffolds indicating that hMSC cells were highly active on the conductive scaffolds, which may be due to the improved intracellular electrical signaling among the cells.

The structure of the scaffolds is suitable for bone cell growth. The porosity of ~60% with the pore size of 50–300 μm provides a large surface area for cell growth and sufficient volume for cell mass. The size of the pores and their interconnectivity can facilitate diffusion of nutrients in and metabolic wastes out of the scaffold, which has been shown to increase the metabolic activity of osteoblast cells.[43–45] The potential for osteoblast ingrowth to the scaffold has been previously shown to cause mechanical bonding between natural bone and the scaffold. This bonding leads to biological fixation of the scaffold in the nonunion part of the fracture and eventual biodegradation and substitution with the host bone.[44]

It is expected that BaG/Gel/PEDOT:PSS show high bioactivity and bond formation to natural bone. The glassy nature of BaG and its composition are two crucial factors for bioactivity of this material.[29] According to these factors and the proven glassy nature of the authors' BaG using XRD, the scaffolds should bond to bone and not to soft tissue.[29] When BaG composites are in contact with body fluid, a layer of hydroxyapatite with incorporated collagen molecules forms on the surface which makes a biological bonding with the natural bone.[28,29,46]

The mechanical properties indicate that the BaG/Gel/PEDOT:PSS nanocomposites could possibly resist in vivo mechanical stresses when placed in the body. Based on the obtained results, having PEDOT:PSS in the composition of bone scaffolds can offer significant enhancement in their mechanical properties. This effect is in agreement with the other characterization results such as biodegradation, DSC analysis, and NMR spectra that suggest a more stable structure for the composites containing PEDOT:PSS.

The influence of PEDOT:PSS was very significant in the in vitro enzyme degradation resistance of the scaffolds. The weight loss or degradation rate was defined as a measure to show what percent of the original scaffold materials were left in the bulk of the scaffold after a certain period of time. In these experiments, it was observed that the materials left the scaffold bulk by enzymatic digestion (dissolution to the surrounding solution) or by producing isolated BaG particles in the solution. Based on the authors' observations, isolated particles rarely formed in scaffolds containing PEDOT:PSS, which indicates the coherence and stability of these scaffolds due to the bonds between PEDOT:PSS and polypeptides chains which were also shown in NMR analysis. As can be seen in Figure 8B, the scaffolds without PEDOT had a weight loss of 70% after 1 day. These scaffolds were completely collapsed after 10 days. The degradation of 0.1 P and 0.3 P were almost similar. They lost about 10%, 20%, 25%, and 35% of their weight after 10, 20, 40, and 90 days immersion in enzyme solution. This can be an especially promising result for large bone defects in which more time is required for the healing process.

PEDOT presents very low intrinsic cytotoxicity and inflammatory response during in vivo examinations. Enzymatic degradation of PEDOT:PSS is not expected as it does not have bio-origin and its structure is chemically stable.[47] The residuals of PEDOT:PSS can be collected and disposed of by the human body. Generally, large molecules of water soluble synthetic polymers can remain in tissue and return to the blood stream by lymphatic circulation.[48] If the molecules are under the glomerular threshold, they will be eliminated by glomerular filtration in the kidneys and will be excreted in the urine. The polymeric chains larger than the renal threshold may be taken by the mononuclear phagocyte system, also known as reticuloendothelial system, as a foreign material.[48–50] After phagocytosis, the synthetic polymer will be destroyed or sequestered in mononuclear phagocyte system organs. Also the pathway of excreting PEDOT:PSS can be a xenobiotic metabolism in the liver.[51,52] The accumulation of synthetic polymers in mononuclear phagocyte system organs, such as the liver and spleen, can have negative side effects; however, with the small amount of PEDOT:PSS used in the conductive scaffold, this issue may not be a problem.[53] Inorganic components of BaG, including

calcium, phosphorous, and silicon – which are bioactive minerals that exist in the inorganic structure of natural bone,[29] are osteoproductive and osteoconductive.

Based on the results in this study, the BaG/Gel/PEDOT:PSS scaffold is physicochemically stable and may mimic the liabilities of spongy bone in the body. It has more appropriate characteristics for cell adhesion and migration compared to the similar scaffolds with no PEDOT:PSS content.

The influence of conductive scaffolds on the cell growth can also be considered as a possible motive on the improvement of the electrical signaling among cells. Based on Nernst's second law, there is a correlation between the membrane voltage of a cell (potential across cell membrane) and the ion flux across the membrane of that cell.[54] This ion flow is the source of a small current with specific velocity that can adjust the cell membrane voltage.[55] And in a reciprocal relationship, the induced voltage can regulate the ion flow.[55,56]

An electric field can be formed in a polarized cell membrane, which can influence the voltage and ion flux of the adjacent cells so that cells can act in correlation.[55–57] The conductivity of the scaffold facilitates such electrical communication among cells. Since ion flux of cells has influence on the general cell performances such as cell attachment, viability, and migration, it is expected that employing conductive scaffolds influences cell response and viability.

It is anticipated that if the conductive scaffold were to be employed for bone healing in actual in vivo experiments by applying electric/magnetic stimuli, it is expected that employing conductive scaffolds influences cell response and viability.

Healing time is a key factor in treating large bone defects. The period of large bone fracture healing can be from several weeks to 2 years.[58,59] When the healing time is extended, there is a risk that the fractures will not join properly (nonunion fractures).[58,59] Due to the high demand for decreasing the duration of fracture healing and enhancing the quality of bone healing and fracture fusions, several strategies have been developed including employing electromagnetic stimuli.[58,61] For this purpose, the scaffolds are required to be conductive to locally deliver the electromagnetic stimuli to the site of the injury. Although the electromagnetic stimuli was not used in this paper, it is an important subject for the authors' future studies (both in vitro and in vivo) and it is hypothesized that this technique may make the tissue engineering methods applicable for large bone defects.

Conclusion

Electrically conductive bioceramic scaffolds were synthesized by combination conductive PEDOT:PSS, Gel, and BaG aiming to combine application of electrical stimuli and 3D bone scaffolding for the enhancement of the bone healing process. Material characterizations indicated that PEDOT:PSS and polypeptide chains can form salt bridges between arginine side chains and sulfonate groups, which may be responsible for the improved stability of the scaffolds. This stability enhanced mechanical properties and in vitro enzyme degradation resistance, providing an appropriate degradation rate for bone healing. Cell culture results indicate that this nanocomposite scaffold is biocompatible and can support hMSC growth. The cell viability increased by increasing the amount of CP in the scaffold composition. Application of electrical stimuli to study the influence of the scaffolds' conductivity in bone healing is targeted for future works.

Acknowledgments

The authors would like to acknowledge the funding supports from Interdisciplinary Program in Regenerative Medicine at OSU (IPRMO) through the Provost Office at Oklahoma State University, AFOSR under Grant number FA9550-10-1-0010 and the National Science Foundation under Grant number 0933763.

Disclosure

The authors declare no conflict of interest in this work.

References

1. Fukada E, Yasuda I. On the piezoelectric effect of bone. *J Phys Soc Jpn*. 1957;12(10):1158–1162.
2. Isaacson BM, Bloebaum RD. Bone bioelectricity: what have we learned in the past 160 years? *J Biomed Mater Res A*. 2010;95(4):1270–1279.
3. Ryaby JT. Clinical effects of electromagnetic and electric fields on fracture healing. *Clin Orthop Relat Res*. 1998;(Suppl 355):S205–S215.
4. Bassett CA, Pawluk RJ, Pilla AA. Augmentation of bone repair by inductively coupled electromagnetic fields. *Science*. 1974;184(4136):575–577.
5. Darendeliler MA, Darendeliler A, Sinclair PM. Effects of static magnetic and pulsed electromagnetic fields on bone healing. *Int J Adult Orthodon Orthognath Surg*. 1997;12(1):43–53.
6. Meng S, Rouabhia M, Zhang Z. Electrical stimulation modulates osteoblast proliferation and bone protein production through heparin-bioactivated conductive scaffolds. *Bioelectromagnetics*. 2013;34(3):189–199.
7. Martino CF, Belchenko D, Ferguson V, Nielsen-Preiss S, Qi HJ. The effects of pulsed electromagnetic fields on the cellular activity of SaOS-2 cells. *Bioelectromagnetics*. 2008;29(2):125–132.
8. Ozawa H, Abe E, Shibasaki Y, Fukuhara T, Suda T. Electric fields stimulate DNA synthesis of mouse osteoblast-like cells (MC3T3-E1) by a mechanism involving calcium ions. *J Cell Physiol*. 1989;138(3):477–483.
9. Wang Z, Clark CC, Brighton CT. Up-regulation of bone morphogenetic proteins in cultured murine bone cells with use of specific electric fields. *J Bone Joint Surg Am*. 2006;88(5):1053–1065.

10. Torricelli P, Fini M, Giavaresi G, Botter R, Beruto D, Giardino R. Biomimetic PMMA-based bone substitutes: a comparative in vitro evaluation of the effects of pulsed electromagnetic field exposure. *J Biomed Mater Res A*. 2003;64(1):182–188.
11. Meng S, Zhang Z, Rouabhia M. Accelerated osteoblast mineralization on a conductive substrate by multiple electrical stimulation. *J Bone Miner Metab*. 2011;29(5):535–544.
12. Munch E, Franco J, Deville S, Hunger P, Saiz E, Tomsia AP. Porous ceramic scaffolds with complex architectures. *JOM (1989)*. 2008;60(6):54–58.
13. Chen QZ, Thompson ID, Boccaccini AR. 45S5 Bioglass-derived glass–ceramic scaffolds for bone tissue engineering. *Biomaterials*. 2006;27(11):2414–2425.
14. Yoshikawa H, Myoui A. Bone tissue engineering with porous hydroxyapatite ceramics. *J Artif Organs*. 2005;8(3):131–136.
15. Guimard NK, Gomez N, Schmidt CE. Conducting polymers in biomedical engineering. *Prog Polym Sci*. 2007;32:876–921.
16. Mozafari M, Mehraien M, Vashaee D, Tayebi L. Electroconductive nanocomposite scaffolds: a new strategy into tissue engineering and regenerative medicine. In: Ebrahimi F, editor. *Nanocomposites: New Trends and Developments*. Rijeka: InTech; 2012:369–392.
17. Li MY, Guo Y, Wei Y, MacDiarmid AG, Lelkes PI. Electrospinning polyaniline-contained gelatin nanofibers for tissue engineering applications. *Biomaterials*. 2006;27(13):2705–2715.
18. Shao S, Zhou S, Li L, et al. Osteoblast function on electrically conductive electrospun PLA/MWCNTs nanofibers. *Biomaterials*. 2011;32(11):2821–2833.
19. Supronowicz PR, Ajayan PM, Ullmann KR, Arulanandam BP, Metzger DW, Bizios R. Novel current-conducting composite substrates for exposing osteoblasts to alternating current stimulation. *J Biomed Mater Res*. 2002;59(3):499–506.
20. Liu Y, Cui H, Zhuang X, et al. Nano-hydroxyapatite surfaces grafted with electroactive aniline tetramers for bone-tissue engineering. *Macromol Biosci*. 2013;13(3):356–365.
21. Cui H, Liu Y, Deng M, et al. Synthesis of biodegradable and electroactive tetraaniline grafted poly(ester amide) copolymers for bone tissue engineering. *Biomacromolecules*. 2012;13(9):2881–2889.
22. Luo SC, Ali EM, Tansil NC, et al. Poly(3,4-ethylenedioxythiophene) (PEDOT) nanobiointerfaces: thin, ultrasmooth, and functionalized PEDOT films with in vitro and in vivo biocompatibility. *Langmuir*. 2008;24(15):8071–8077.
23. Kim DR, Abidian M, Martin D. Synthesis and characterization of conducting polymers grown in hydrogels for neural applications. In: Wong JY, Plant AL, Schmidt CE, et al, editors. *Architecture and Application of Biomaterials and Biomolecular Materials*, *Boston*, *MA*, *December 1–4, 2003*. Warrendale, PA: Materials Research Society; 2004:55–60.
24. Groenendaal L, Jonas F, Freitag D, Pielartzik H, Reynolds JR. Poly(3,4-ethylenedioxythiophene) and its derivatives: past, present, and future. *Adv Mater*. 2000;12(7):481–494.
25. Schweizer TM. *Electrical Characterization and Investigation of the Piezoresistive Effect of PEDOT:PSS Thin Films [Master's Thesis]*. Atlanta, GA: Georgia Institute of Technology; 2005.
26. Wu X, Liu Y, Li X, et al. Preparation of aligned porous gelatin scaffolds by unidirectional freeze-drying method. *Acta Biomater*. 2010;6(3):1167–1177.
27. Mao JS, Zhao LG, Yin YJ, Yao KD. Structure and properties of bilayer chitosan–gelatin scaffolds. *Biomaterials*. 2003;24(6):1067–1074.
28. Mozafari M, Rabiee M, Azami M, Maleknia S. Biomimetic formation of apatite on the surface of porous gelatin/bioactive glass nanocomposite scaffolds. *Appl Surf Sci*. 2010;257(5):1740–1749.
29. Cerruti MG. *Characterization of Bioactive Glasses. Effect of the Immersion in Solutions That Simulate Body Fluids [PhD Thesis]*. Turin: University of Turin; 2004.
30. Kozielski M, Buchwald T, Szybowicz M, Blaszczak Z, Piotrowski A, Ciesielczyk B. Determination of composition and structure of spongy bone tissue in human head of femur by Raman spectral mapping. *J Mater Sci Mater Med*. 2011;22(7):1653–1661.
31. Mozafari M, Moztarzadeh F, Rabiee M, et al. Development of macroporous nanocomposite scaffolds of gelatin/bioactive glass prepared through layer solvent casting combined with lamination technique for bone tissue engineering. *Ceramics International*. 2010;36(8):2431–2439.
32. Mozafari M, Moztarzadeh F, Tahriri M. Investigation of the physicochemical reactivity of a mesoporous bioactive SiO_2–CaO–P_2O_5 glass in simulated body fluid. *J Non Cryst Solids*. 2010;356(28–30):1470–1478.
33. Timkovich R. Detection of the stable addition of carbodiimide to proteins. *Anal Biochem*. 1977;79(1–2):135–143.
34. Wu L, Zhang H, Zhang J, Ding J. Fabrication of three-dimensional porous scaffolds of complicated shape for tissue engineering. I. Compression molding based on flexible-rigid combined mold. *Tissue Eng*. 2005;11(7–8):1105–1114.
35. Yin K, Zhu Z. "One-pot" synthesis, characterization, and NH_3 sensing of Pd/PEDOT:PSS nanocomposite. *Synth Met*. 2010;160(9–10):1115–1118.
36. Seo KI, Chung IJ. Reaction analysis of 3,4-ethylenedioxythiophene with potassium persulfate in aqueous solution by using a calorimeter. *Polymer*. 2000;41(12):4491–4499.
37. Iyer P, Walker KJ, Madihally SV. Increased matrix synthesis by fibroblasts with decreased proliferation on synthetic chitosan–gelatin porous structures. *Biotechnol Bioeng*. 2012;109(5):1314–1325.
38. Crispin X, Marciniak S, Osikowicz W, et al. Conductivity, morphology, interfacial chemistry, and stability of poly(3,4-ethylene dioxythiophene)–poly(styrene sulfonate): a photoelectron spectroscopy study. *J Polym Sci B Polym Phys*. 2003;41(21):2561–2583.
39. Timpanaro S, Kemerink M, Touwslager FJ, De Kok MM, Schrader S. Morphology and conductivity of PEDOT/PSS films studied by scanning–tunneling microscopy. *Chem Phys Lett*. 2004;394(4–6):339–343.
40. Adriaensens P, Carleer R, Storme L, Vanderzande D, Gelan J. Morphological study of a poly(3,4-ethylenedioxythiophene)/polystyrenesulfonic acid mixture by solid state ^{13}C-CP/MAS NMR relaxometry. *Polymer*. 2002;43(25):7003–7006.
41. Donald JE, Kulp DW, DeGrado WF. Salt bridges: geometrically specific, designable interactions. *Proteins*. 2011;79(3):898–915.
42. Russell VA, Etter MC, Ward MD. Guanidinium parasubstituted benzenesulfonates: competitive hydrogen bonding in layered structures and the design of nonlinear optical materials. *Chem Mater*. 1994;6(8):1206–1217.
43. Salgado AJ, Coutinho OP, Reis RL. Bone tissue engineering: state of the art and future trends. *Macromol Biosci*. 2004;4(8):743–765.
44. Yang S, Leong KF, Du Z, Chua CK. The design of scaffolds for use in tissue engineering. Part 1. Traditional factors. *Tissue Eng*. 2001;7(6):679–689.
45. Whang K, Healy KE, Elenz DR, et al. Engineering bone regeneration with bioabsorbable scaffolds with novel microarchitecture. *Tissue Eng*. 1999;5(1):35–51.
46. Perez-Pariente J, Balas F, Roman J, Salinas AJ, Vallet-Regi M. Influence of composition and surface characteristics on the in vitro bioactivity of SiO_2–CaO–P_2O_5–MgO sol–gel glasses. *J Biomed Mater Res*. 1999;47(2):170–175.
47. Peramo A, Urbanchek MG, Spanninga SA, Povlich LK, Cederna P, Martin DC. In situ polymerization of a conductive polymer in acellular muscle tissue constructs. *Tissue Eng Part A*. 2008;14(3):423–432.
48. Markovsky E, Baabur-Cohen H, Eldar-Boock A, et al. Administration, distribution, metabolism and elimination of polymer therapeutics. *J Control Release*. 2012;161(2):446–460.
49. Domb AJ, Kumar N, Ezra A, editors. Chapter 16 in *Biodegradable Polymers in Clinical Use and Clinical Development*. Hoboken, NJ: John Wiley & Sons; 2011.
50. Kadajji VG, Betageri GV. Water soluble polymers for pharmaceutical applications. *Polymers*. 2011;3(4):1972–2009.
51. Omiecinski CJ, Vanden Heuvel JP, Perdew GH, Peters JM. Xenobiotic metabolism, disposition, and regulation by receptors: from biochemical phenomenon to predictors of major toxicities. *Toxicol Sci*. 2011;120(Suppl 1):S49–S75.

52. Coleman MD. *Human Drug Metabolism: An Introduction*. Hoboken, NJ: John Wiley & Sons; 2005.
53. Owens DE 3rd, Peppas NA. Opsonization, biodistribution, and pharmacokinetics of polymeric nanoparticles. *Int J Pharm*. 2006;307(1):93–102.
54. Buck RP. Kinetics of bulk and interfacial ionic motion: microscopic bases and limits for the nernst–planck equation applied to membrane systems. *J Memb Sci*. 1984;17(1):1–62.
55. Levin M. Large-scale biophysics: ion flows and regeneration. *Trends Cell Biol*. 2007;17(6):261–270.
56. Levin M. Bioelectric mechanisms in regeneration: unique aspects and future perspectives. *Semin Cell Dev Biol*. 2009;20(5):543–556.
57. Levin M. Bioelectromagnetics in morphogenesis. *Bioelectromagnetics*. 2003;24(5):295–315.
58. Peres JA, Lamano T. Strategies for stimulation of new bone formation: a critical review. *Braz Dent J*. 2011;22(6):443–448.
59. Antonova E, Le TK, Burge R, Mershon J. Tibia shaft fractures: costly burden of nonunions. *BMC Musculoskelet Disord*. 2013;14:42.
60. Galkowski V, Petrisor B, Drew B, Dick D. Bone stimulation for fracture healing: what's all the fuss? *Indian J Orthop*. 2009;43(2):117–120.
61. Rose PI, Gross S. High-resolution proton magnetic resonance studies of gelatin solution and gels. *Journal of Photographic Science*. 1975;23(2):59–67.